

A Lattice Boltzmann solver for Maxwell equations in dielectric media

S.A. Galindo-Torres, A Scheuermann

Geotechnical Engineering Centre, School of Civil Engineering, The University of Queensland, Brisbane QLD 4072, Australia

Research Group of Complex Processes in Geo-Systems, School of Civil Engineering, The University of Queensland, Brisbane QLD 4072, Australia

E-mail: s.galindotorres@uq.edu.au

Ruslan Puscasu

W.H. Bryan Mining and Geology Research Centre, The University of Queensland, Brisbane QLD 4072, Australia

Abstract. Numerical modelling on the interaction between electromagnetic signals and matter is of crucial importance for the formulation of novel inversion algorithms that help in the interpretation of non disruptive scanning methods. One particular problem that is important for the mining sector is the detection of the ore boulder sizes. Such a detection could make the extraction process more efficient. In order to explore this problem a numerical solver for Maxwell equations is presented. The method is based on the Lattice Boltzmann Method. Some validation examples are presented to show that it accurately reproduce the interaction of electromagnetic signals and matter as described in classical electrodynamics. After validation an assembly of two distinct boulder sizes is subjected to a set of propagating electromagnetic signals with different frequencies. The results show how the transmitted signal can offer information on the maximum boulder size. It is expected that this preliminary work will contribute towards better inversion algorithms for electromagnetic prospection methods.

1. Introduction

Electromagnetic prospection methods are becoming more and more popular as a kind of non-disruptive scanning methods. In particular the Ground Penetrating Radar is an useful technique to obtain information on the underground structure [Benter et al.(2009a)Benter, Moore, and Xu]. The advantages of non disruptive methods are clear, since no samples need to be taken and no excavations are needed. However these methods offer also a set of disadvantages mainly in the form of inversion analysis to interpret the signals received.

Numerical modelling can be used as a virtual laboratory to evaluate, in a cost effective way, inversion algorithms. Several algorithms exists to solve the electromagnetic

equations. One popular option involves finite elements [Jin(2014)]. This method has the advantages of a Delaunay partition of space, however it is implicit in nature which limits its parallelization capabilities. Furthermore, one of the main advantages of the triangulation which is having different resolutions in different sub domains, is limited since the elements must be small enough to resolve the smallest wave-length.

Finite Difference Time Domain (FDTD) [Kunz and Luebbers(1993)] and Finite Difference Frequency Domain (FDFD) [Xu et al.(2003)Xu, Zhang, Hong, Wu, and Cui] are also popular methods having some clear advantages over finite elements. Both cases can be explicit, which makes it easier to be solved in a parallel way. Also they can easily deal with a broad range of wave-lengths.

Another alternative that has been growing in popularity lately is the use of the Lattice Boltzmann Method (LBM) as a general partial differential equation solver. Mendoza [Mendoza and Munoz(2010)] introduced its use to solve the macroscopic Maxwell equations in 3D. He has also presented evidence on how it is faster, more memory efficient and requires less resolution than traditional FDTD. Because of these advantages it has been chosen as the method for this work.

The problem that is going to be explored with the method is the detection of boulder sizes in a particle assembly. This particular problem has important application in mining engineering [Benter et al.(2009b)Benter, Xu, Moore, Antolovich, and Gao] where detecting the boulder size distribution a priori can enhance the extraction procedure. In this preliminary work only a very idealistic boulder assembly of two sizes is considered. The results however, as will be seen, are promising showing how a transmitted electromagnetic signal can be used to detect the largest boulder size.

The scope of this paper is as follows: Sec. 2 describes the Electromagnetic Lattice Boltzmann solver (EMLBM). Then some validation examples (Sec. 3) are presented to show how accurately the method reproduces the interaction between electromagnetic waves and matter. Sec. 4 shows the results of electromagnetic propagation signals over the mixed granular assembly. Finally Sec. 5 present the final discussions, conclusions and projections of the current work.

2. The Electromagnetic Lattice Boltzmann Method (EMLBM)

The implementation used for this study is based in the method proposed by Mendoza *et al* [Mendoza and Munoz(2010)]. The method takes a Lattice Boltzmann (LB) grid. This grid discretizes both the space and the velocity spaces. A set of discrete velocities \vec{e}_i connect a given cell with a sub set of neighbour cells. To start describing the method, it is useful to recall the Lattice Boltzmann equation,

$$f_i(\vec{x} + \vec{e}_i, t + \delta_t) = f_i(\vec{x}, t) + \Omega_{col}, \quad (1)$$

which describes how a distribution function f_i evolves for the next time step and how it is streamed over the neighbour cells. For this study, the widely accepted BGK model for the collision operator [Qian et al.(1992)Qian, d'Humieres, and Lallemand] was used,

which assumes that the collision processes drive the system into an equilibrium state described by an equilibrium function f_i^{eq} ,

$$\Omega_{col} = \frac{f_i^{eq} - f_i}{\tau}, \quad (2)$$

where τ is a characteristic relaxation time.

It has been proven [Guangwu(2000)] that this relation can solve a particular set of Partial Differential Equations (PDE) of the form

$$\frac{\partial \vec{\mathbf{A}}}{\partial t} + \nabla \cdot \mathbf{\Pi} = 0, \quad (3)$$

where $\vec{\mathbf{A}}$ is a vector function and $\mathbf{\Pi}$ is a second order tensor and $\tau = 1/2$. The idea behind Mendoza's method is to use LB's PDE solver capability to find approximations to both Ampere's law,

$$\frac{\partial \vec{\mathbf{D}}}{\partial t} - c^2 \nabla \times \vec{\mathbf{H}} + \mu_0 \vec{\mathbf{J}} = 0, \quad (4)$$

and Faraday's law,

$$\frac{\partial \vec{\mathbf{B}}}{\partial t} - \nabla \times \vec{\mathbf{E}} = 0, \quad (5)$$

where $\vec{\mathbf{E}}$ and $\vec{\mathbf{B}}$ are the electric and magnetic field respectively; $\vec{\mathbf{D}} = \epsilon \epsilon_0 \vec{\mathbf{E}}$ and $\mu \mu_0 \vec{\mathbf{H}} = \vec{\mathbf{B}}$ are the displacement and magnetizing field respectively that depend on the vacuum permittivity ϵ_0 and permeability μ_0 and their relative values ϵ and μ . It is easy to see how curl based laws can take the form of Eq. 3 if the curl is represented as the divergence of a tensor,

$$\nabla \times \vec{\mathbf{A}} = \nabla \cdot \begin{bmatrix} 0 & -A_z & A_y \\ A_z & 0 & -A_x \\ -A_y & A_x & 0 \end{bmatrix}. \quad (6)$$

To solve these equations a D3Q13 (3 dimensions 13 velocities) LBM cell division is used. The unit cell is shown in Fig. 1 with each of the 12 vectors $\vec{\mathbf{c}}_i$. For each of these velocities two distribution functions are assigned for the displacement field $d_{ij}, j = 0, 1$ and two for the magnetic field $h_{ij}, j = 0, 1$. Two additional vector sets are required to represent the fields. For instance for vector $\vec{\mathbf{c}}_1 = (\delta_x, \delta_x, 0)$ (δ_x grid size) there is a clockwise vector $\vec{\mathbf{e}}_{1,0} = (-0.5\delta_x, 0.5\delta_x, 0.0)$ and a counter-clockwise vector $\vec{\mathbf{e}}_{1,1} = (0.5\delta_x, -0.5\delta_x, 0.0)$ for the possible electric fields and two vectors for the magnetic field calculation $\vec{\mathbf{b}}_{1,0} = (0, 0, \delta_x)$ and $\vec{\mathbf{b}}_{1,1} = (0, 0, -\delta_x)$. To complete the picture a function representing the rest distributions f_0 is needed.

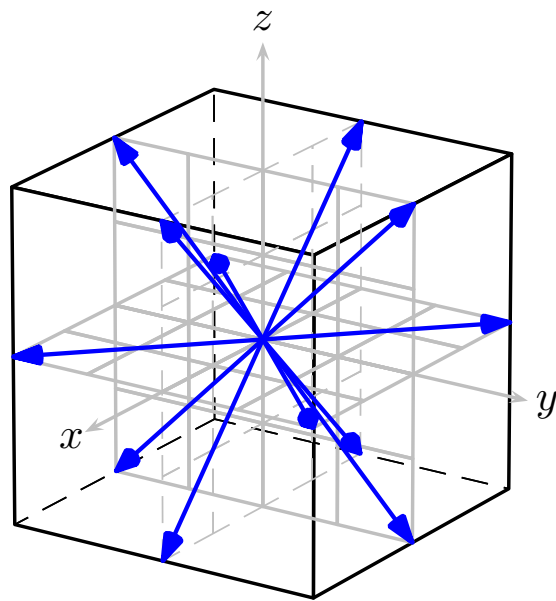


Figure 1. LBM cell showing the direction of the 12 velocities \vec{c}_i including the rest position

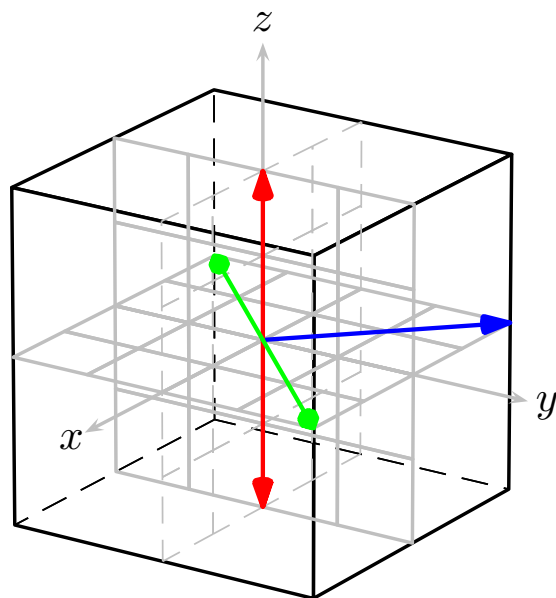


Figure 2. Auxiliary vectors \vec{e}_{ij} (green) and \vec{b}_{ij} (red) associated with a given velocity \vec{c}_i (blue)

The macroscopic fields and charge densities are obtained from the equations,

$$\vec{D} = \sum_{i=1}^{12} \sum_{j=0}^1 d_{ij} \vec{e}_{ij}, \quad (7)$$

$$\vec{B} = \sum_{i=1}^{12} \sum_{j=0}^1 h_{ij} \vec{b}_{ij}. \quad (8)$$

Similarly the charge ρ and current \vec{J} densities are obtained by,

$$\rho = f_0 + \sum_{i=1}^{12} \sum_{j=0}^1 d_{ij} \quad (9)$$

and

$$\vec{J} = \sigma \vec{E}, \quad (10)$$

where the second equation is the definition of Ohm's law with the conductivity σ .

Finally the equilibrium functions for each sub set of distribution functions are given by,

$$d_{ij}^{eq} = \frac{1}{16} \vec{c}_i \cdot \vec{J} + \frac{\epsilon}{4} \vec{E} \cdot \vec{e}_{ij} + \frac{1}{\mu 8} \vec{B} \cdot \vec{b}_{ij} \quad (11)$$

$$h_{ij}^{eq} = \frac{1}{16} \vec{c}_i \cdot \vec{J} + \frac{1}{4} \vec{E} \cdot \vec{e}_{ij} + \frac{1}{8} \vec{B} \cdot \vec{b}_{ij} \quad (12)$$

$$f_0^{eq} = \rho, \quad (13)$$

completing the definition of the Electromagnetic Lattice Boltzmann (EMLBM) solver. A final remark involves the other two Maxwell equations: Gauss law,

$$\nabla \cdot \vec{D} = \rho / \epsilon_0, \quad (14)$$

and the null divergence of the magnetic field,

$$\nabla \cdot \vec{B} = 0. \quad (15)$$

Both equations are equally met as long as the initial conditions over the fields and densities fulfil them.

3. Validation

In order to validate the code to explore its use for the detection of boulder sizes with distinct dielectric constants, two examples taken from Jackson's book [Jackson(1962)] are taken. The first one is an static problem: A dielectric sphere immersed within a dielectric field. The second is a dynamic one: The refraction and reflection of an electromagnetic plane wave trough a dielectric interface.

3.1. Dielectric sphere immersed in uniform electric field

In this first example a dielectric sphere with $\epsilon_{sphere} = 5$ is placed on a domain where an uniform electric field E_0 going in the z direction exists. The domain is composed of $101 \times 101 \times 101$ LBM cells. The sphere rests at the center of the domain and has a radius R of 6 LBM cells. In order to obtain a smooth transition over the interface, the relative permittivity is given by $\epsilon = \epsilon_{sphere}\gamma$ where γ is the volume fraction of a cell occupied by the sphere. It is clear that for the cells inside the sphere $\gamma = 1$ and outside $\gamma = 0$. Only on the interface γ takes intermediate values. The calculation of γ was carried out by the fast algorithm proposed by the author [Galindo-Torres(2013a)].

By experimentation it was found that setting the an uniform field at the beginning did not work for this example. The best initial condition was to set the electric field as zero in all the domain except for the boundary $x = 0$ and $x = 100$ where an uniform electric field was imposed by setting the distribution functions of these cells as the equilibrium values. The wave propagates until the full domain is filled with the uniform electric field deformed by the dielectric sphere. The simulation ran for 5000 iterations until a time independent configuration was reached.

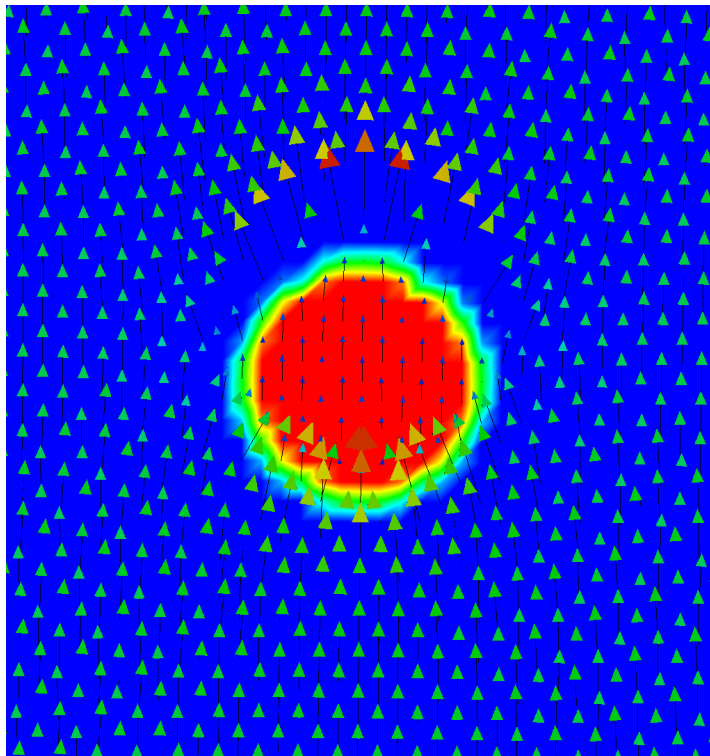


Figure 3. Cross section plane of an electric field (arrows) in the presence of dielectric sphere (colormap)

Fig. 3 shows the final electric field distribution. Far from the sphere the field is uniform but close to it the electric field is deformed by going into and out from the sphere and by having a constant value inside it. An analytical closed-form solution exists for

the electric field as a function of x for a line starting at the sphere center [Jackson(1962)],

$$E_{inside} = \frac{2E_0}{\epsilon + 2} \quad (16)$$

$$E_{out} = E_0 \left[1 - \frac{\epsilon - 1}{\epsilon + 2} \left(\frac{R}{x} \right)^3 \right]. \quad (17)$$

The comparison of the formula with the obtained results is shown in Fig. 4 where a good match is found, albeit with the presence of numerical noise. This validation example fixes a lower bound for the resolution needed to represent a dielectric sphere.

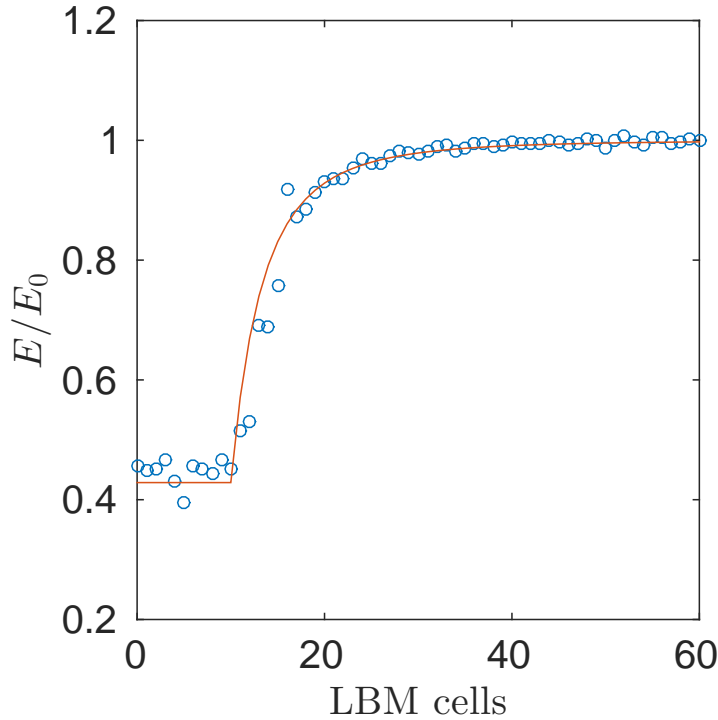


Figure 4. Electric field as a function of x in the presence of a dielectric sphere. The sudden change occurs at the radius of the sphere equal to 6 LBM cells

3.2. Snell's law

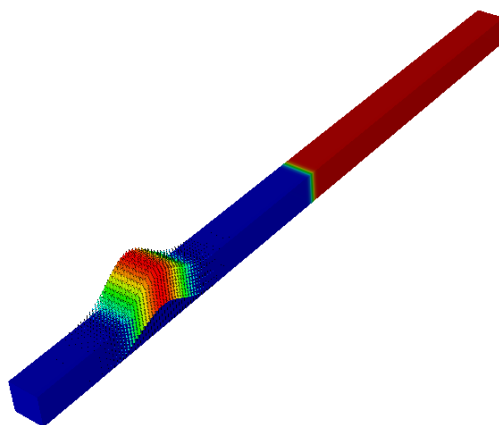
The second example involves the dynamic refraction and reflection of an electromagnetic plane wave across a dielectric interface in complete analogy with the example prepared by Mendoza *et al* [Mendoza and Munoz(2010)]. An array of 10x10x200 LBM cells was fixed and each cell was assigned a value for ϵ given by $2.0 * \tanh(z - 100) + 3.0$. Therefore before the value $z = 100$ the medium has a permittivity of 1 and after this value it has a value of 5. The plane wave is modelled by a Gaussian package for the electric field E on the x direction,

$$E_0 \exp\left(-0.01(z - 40)^2\right), \quad (18)$$

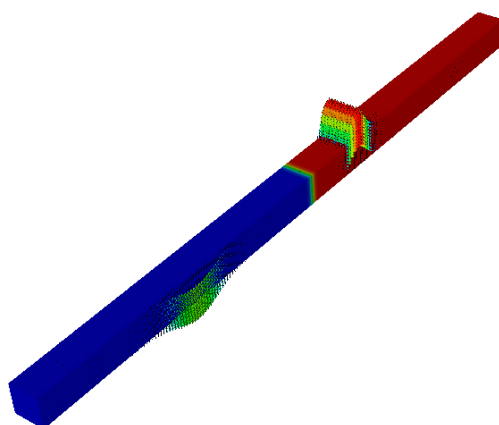
and a similar expression for the magnetic field in the y direction

$$B_0 \exp\left(-0.01(z - 40)^2\right), \quad (19)$$

where $B_0 = E_0/c$ and $c = 1/\sqrt{2}$ is the speed of light in LBM units. With this initial condition of electric and magnetic fields it is guaranteed that the pulse will propagate in the z direction.



(a)



(b)

Figure 5. Initial (a) and final (b) pulse (vectors) propagating across a dielectric interface (colormap).

Fig. 5 shows the initial and final electric field distributions. In the final stage the pulse is divide in two, one propagating through to dielectric medium and one being

reflected. Again there are closed-form solutions for the amplitude of both the refracted

$$E_{refracted} = \frac{2E_0}{\sqrt{\epsilon + 1}}, \quad (20)$$

and reflected

$$E_{reflected} = E_0 \frac{\sqrt{\epsilon} - 1}{\sqrt{\epsilon} + 1} \quad (21)$$

electric fields.

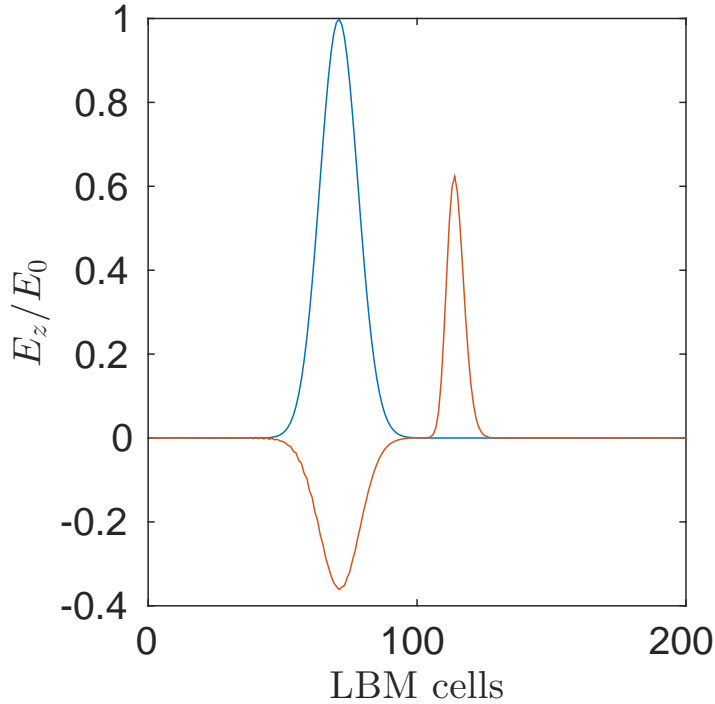


Figure 6. Initial (blue) and final (red) electric amplitudes

Fig. 6 shows the initial and final electric amplitudes. The simulation results are $E_{refracted}/E_0 = 0.6236$ and $E_{reflected}/E_0 = -0.3711$ to be compared with the theoretical values 0.6180 and -0.3820 respectively. This shows a proper interaction between dielectric matter and electromagnetic waves which is critical for the future analysis presented in this paper.

4. Boulder size detection

An assembly of two sphere sizes (5m and 1m) was randomly distributed over the space and compressed by using the Discrete Element Method as described in [Galindo-Torres(2013b)]. The relative permittivity $\epsilon = 5$ for all boulders. Once the compressed sample is obtained, one plate antenna covering the whole left boundary is simulated by an harmonic electric field which propagates across. Before the sample there is a space of 10 LBM cells and after it there are 100 LBM cells. The reason

there is a large buffer at the end is to prevent the right boundary to affect the measured signal. The smallest particle size is resolved with 10 cells (so $\delta_x = 0.1m$) which has been proven in the validation examples to be enough resolution to represent the interaction with matter.

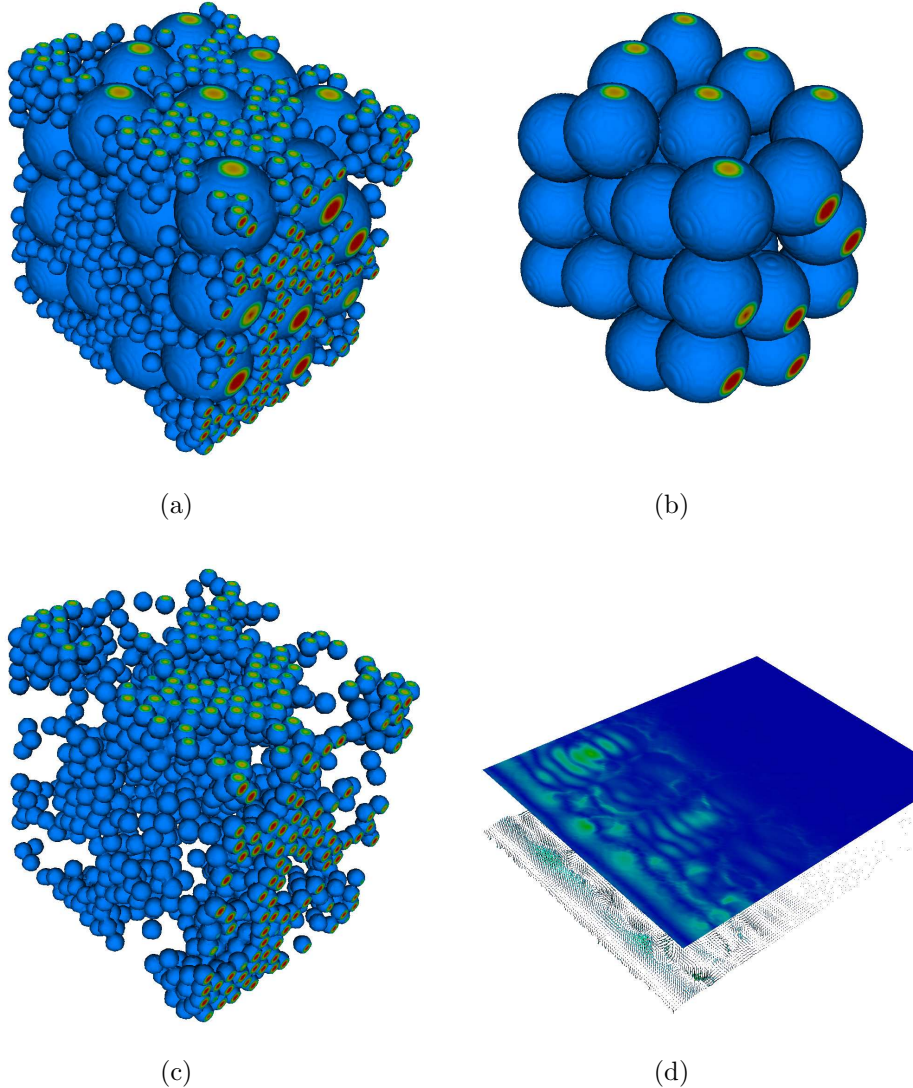


Figure 7. a) The whole boulder assembly; b) only the large particles; c) only the small ones; d) a cross section showing the electric field propagating across the sample (colormap and vector)

Fig 7(a) shows the mixed assembly which is distributed randomly. Similarly Fig. 7(d) shows the electric field intensity propagating across the sample. Four different wave-lengths were considered: 2m, 4m, 6m and 8m. Assuming that the speed of light is $c = 3 \times 10^8 \text{m/s}$ these values represent frequencies of 150, 75, 50 and 37.5 MHz which are signals commonly used in Ground Penetrating Radar (GPR) measurements [Benter et al.(2011)Benter, Antolovich, and Moore].

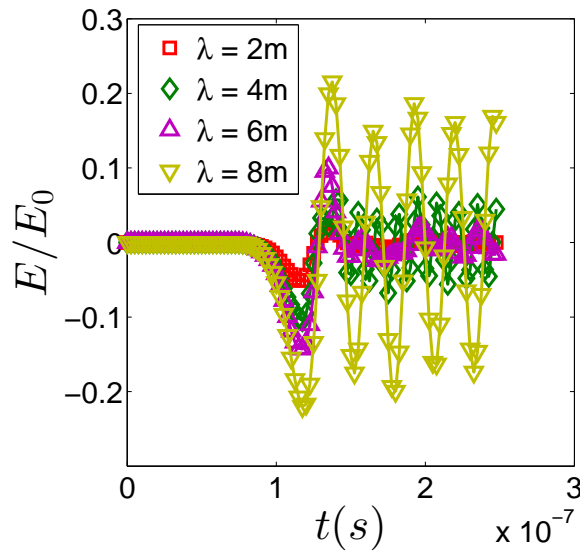


Figure 8. Transmitted signal obtained at the right plate.

The measured signal at the end of the sample, obtained by averaging the electric field at the right plate roughly 200 cells from the left boundary and 100 cells from the right one, is shown in Fig. 8. As can be seen higher wave-lengths do not have as many signal losses as smaller ones. Also, regardless of the frequency, there appears to be an underlying wave added to the signal which seems to be the same for all the wave-lengths considered.

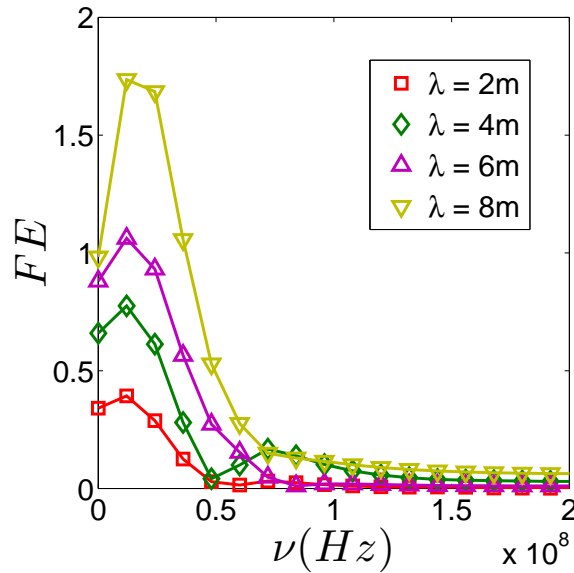


Figure 9. Fourier amplitude (FE) for different frequencies

Fourier analysis is needed to observe the contribution of the different signals into the transmitted one. Fig. 9 shows the Fourier amplitude (as the absolute value of the

Fourier coefficient) for different frequencies. There is a clear signal of 12 MHz for all wave-lengths which is the most important, overshadowing even the induced signal. This frequency is equivalent to a wave-length of 25m or roughly five time the diameter of the largest boulder.

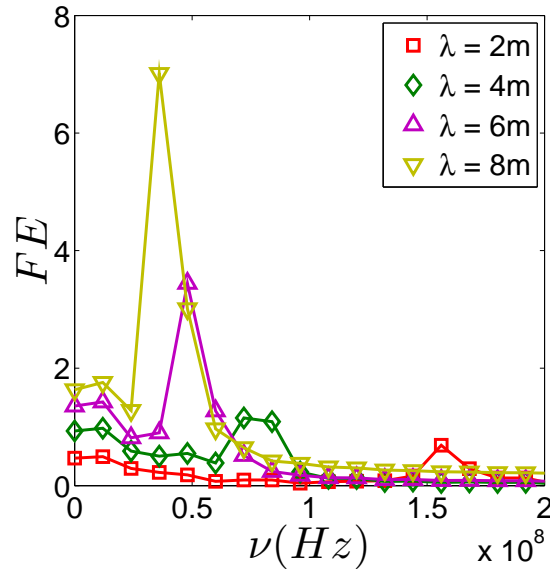


Figure 10. Fourier amplitude (FE) for different frequencies for only the smallest particles.

Numerical modelling allows for the exploration of features that are very difficult to observe in reality. For instance, the different groups of particles can be erased and their contributions to the transmitted signals are able to be studied independently. Fig. 10 shows the transmitted signal when only the small boulders are considered as in Fig. 7(c). The signal shows a contribution from the induced frequencies with the four peaks clearly shown at the values imposed at the left boundary. Again it can be seen that the signal has higher losses as the wave-length is smaller. The peak at 12MHz is not as evident as in the case of the mixed assembly. It may be concluded that the smallest particles are not the main contributors to this underlying signal.

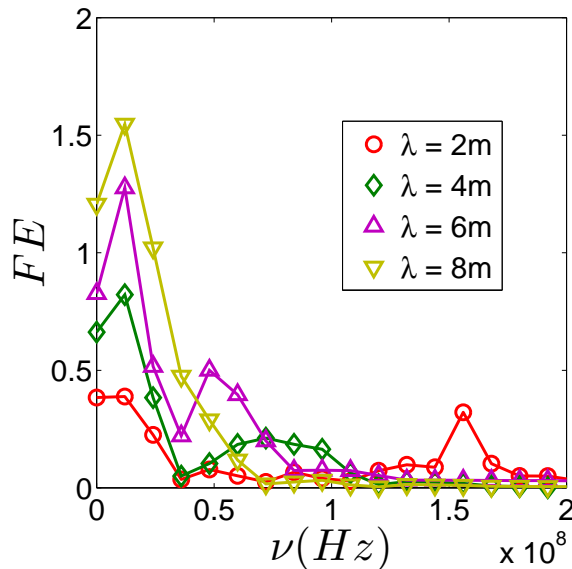


Figure 11. Fourier amplitude (FE) for different frequencies for only the largest particles.

Now only the largest particles are considered as in Fig. 7(b). Fig. 11 shows the Fourier amplitude for the largest boulders. As can be seen the signal of 12MHz is clear and the spectra resembles the case of the whole assembly. Even the losses (by the magnitude of FE) are similar to the mixed case. Therefore, the large boulders are the ones producing the 12MHz and the overall signal loss on the transmission.

5. Discussion and conclusions

A numerical solver for Maxwell equation's within dielectric media is presented. The implementation is based on Mendoza's *et al* [Mendoza and Munoz(2010)] method. It uses the Lattice Boltzmann Method and therefore is named Electromagnetic Lattice Boltzmann (EMLBM) solver.

Two validation examples are presented to show how the interaction between electromagnetic fields and matter is accurately captured with the method. The first one is the static problem of a dielectric sphere immersed in a uniform electric field. Although the results present some numerical noise, this example shows that a sphere can be represented by 10 LBM cells covering its diameter.

The second example is a simplified version of Snell's law for refraction. The accuracy of the results show that the model is able to cope with the interaction of matter and electromagnetic waves.

After validation a systematic simulation plan involving a granular assembly involving two distinct boulder sizes (1m and 5m) is carried out. The results show a clear signal of 12MHz that overshadows even the induced signal. Thanks to the virtual nature of this numerical experimentation, the contributions from each grain size can be

observed independently. First the large boulders are erased from the assembly. The signal shows the peaks corresponding to the induced frequencies. Therefore the small boulders are not responsible for the observed anomalous signal.

By filtering now the contribution of the small boulders the anomalous 12MHz is clearly seen. In fact the signal of just the largest boulders is strikingly similar to the signal for the mixed assembly. It can be said then that the large boulders produce reflections that are responsible for the 12MHz signal. The wave-length of the signal (25m) is roughly 5 times the diameter of the large boulder which could potentially be used to detect this maximum boulder size.

Further studies are needed to elucidate the contribution of broader distributions of boulder sizes. Also DEM capabilities with particles of general shapes could be used to study realistic boulder geometries as seen in Ref [Galindo-Torres(2013b)]. Similarly more realistic values for the conductivity (here taken as 0) and permeability must be taken to account for metallic ores.

Acknowledgements

The simulations were carried out with the EMLBM module of the MechSys open source library (<http://mechsys.nongnu.org/index.shtml>). The Macondo High Performance Computing Cluster, hosted by the School of Civil Engineering at UQ, was used to ran the simulation plan.

References

- [Benter et al.(2009a)Benter, Moore, and Xu] A. Benter, W. Moore, and R. Xu, in *Australian Mining Technology Conference. CRC Mining* (2009a).
- [Jin(2014)] J. Jin, *The finite element method in electromagnetics* (John Wiley & Sons, 2014).
- [Kunz and Luebbers(1993)] K. S. Kunz and R. J. Luebbers, *The finite difference time domain method for electromagnetics* (CRC press, 1993).
- [Xu et al.(2003)Xu, Zhang, Hong, Wu, and Cui] F. Xu, Y. Zhang, W. Hong, K. Wu, and T. J. Cui, *Microwave Theory and Techniques*, IEEE Transactions on **51**, 2221 (2003).
- [Mendoza and Munoz(2010)] M. Mendoza and J. Munoz, *Physical Review E* **82**, 056708 (2010).
- [Benter et al.(2009b)Benter, Xu, Moore, Antolovich, and Gao] A. Benter, R. Xu, W. Moore, M. Antolovich, and J. Gao, in *Radar Conference-Surveillance for a Safer World, 2009. RADAR. International* (IEEE, 2009b), pp. 1–5.
- [Qian et al.(1992)Qian, d’Humieres, and Lallemand] Y. Qian, D. d’Humieres, and P. Lallemand, *EPL (Europhysics Letters)* **17**, 479 (1992).
- [Guangwu(2000)] Y. Guangwu, *Journal of Computational Physics* **161**, 61 (2000).
- [Jackson(1962)] J. D. Jackson, *Classical electrodynamics*, vol. 3 (Wiley New York etc., 1962).
- [Galindo-Torres(2013a)] S. Galindo-Torres, *Computer Methods in Applied Mechanics and Engineering* **265**, 107 (2013a), ISSN 0045-7825.
- [Galindo-Torres(2013b)] S. Galindo-Torres, *Granular Matter* pp. 1–12 (2013b), ISSN 1434-5021, URL <http://dx.doi.org/10.1007/s10035-013-0428-6>.
- [Benter et al.(2011)Benter, Antolovich, and Moore] A. Benter, M. Antolovich, and W. Moore, in *Advanced Ground Penetrating Radar (IWAGPR), 2011 6th International Workshop on* (IEEE, 2011), pp. 1–6.